8-2016

AN AUTOMATED SYRINGE PUMP SYSTEM FOR IMPROVING THE REPRODUCIBILITY OF DYNAMIC HYPERPOLARIZED MRI PHANTOMS

Harlee G. Harrison

AN AUTOMATED SYRINGE PUMP SYSTEM FOR IMPROVING THE

REPRODUCIBILITY OF DYNAMIC HYPERPOLARIZED MRI PHANTOMS

By

Harlee Grace Harrison, B.S.

APPROVED:

James Bankson, Ph.D., Advisory Professor

Jason Stafford, Ph.D.

Donna Reeve, M.S.

Arvind Rao, Ph.D.

David Followill, Ph.D.

APPROVED:

Dean, The University of Texas

Graduate School of Biomedical Sciences at Houston

AN AUTOMATED SYRINGE PUMP SYSTEM FOR IMPROVING THE REPRODUCIBILITY OF DYNAMIC HYPERPOLARIZED MRI PHANTOMS

THESIS

Presented to the Faculty of

The University of Texas

Health Science Center at Houston

and

The University of Texas

M.D. Anderson Cancer Center

Graduate School of Biomedical Sciences

in Partial Fulfillment

of the Requirements

for the Degree of

MASTER OF SCIENCE

By

Harlee Grace Harrison, B.S.

Houston, Texas

August, 2016

Dedication

To my dad, for always reminding me to whip it, whip it good.

Acknowledgements

I cannot express enough gratitude to my committee for guiding me through this learning process: Dr. James Bankson, my committee chair; Dr. Jason Stafford; Ms. Donna Reeve; Dr. Arvind Rao; and Dr. David Followill. I sincerely appreciate all of the guidance and learning opportunities that each of you provided to me.

I would like to express thanks to Chris Walker, without whom this this work could not have been completed, and to Daniela Branco, for keeping me sane along the way. I would also like to express gratitude to Ms. Betsy Kindred and Dr. Richard Wendt III, for being advocates for me and all other students along the way.

I also could not have made it through this work without the support of my mother, Jayna Harrison, and father, Mike Harrison, who always believe in me. I would also like to thank my loving husband, Preston Griffin, who has been my place of rest no matter how stressful life gets. I will always be grateful for your love and support.

Finally I would like to thank God for bringing me get this far. I could not have made it with my own strength, but "I can do all things through Christ who strengthens me."

AN AUTOMATED SYRINGE PUMP SYSTEM FOR IMPROVING THE REPRODUCIBILITY OF DYNAMIC HYPERPOLARIZED MRI PHANTOMS

Harlee Grace Harrison, B.S.

Advisory Professor: James Bankson, Ph.D.

Magnetic Resonance Imaging (MRI) is a powerful tool in the diagnosis of cancer due to its ability to provide good soft tissue contrast and image resolution without the use of ionizing radiation. The use of hyperpolarized pyruvate as a contrast agent for tumor metabolism during MR scans has the potential to provide information about tumor metabolism in vivo that is not available from traditional imaging measurements or any other method. Hyperpolarization is achieved through dynamic nuclear polarization. This is a process in which a sample is quickly frozen to near absolute zero (~1.4K), and placed in a strong magnetic field. In these conditions, magnetization in unpaired electrons, in this case from a Trityl radical, can convey their polarization to a nearby ^{13}C nucleus through microwave irradiation. Pyruvate, which plays a central role in metabolism, is involved in aerobic glycolysis, a primary energy pathway for cancer cells. In this process, known as the Warburg effect, the up-regulation of lactate dehydrogenase leads to the increased chemical conversion of pyruvate to lactate. Due to the conservation of hyperpolarized ^{13}C-enriched pyruvate's nuclear spin state through chemical conversion, the signal from pyruvate and metabolites such as lactate can be observed. Although the signal is largely increased, this improvement is short lived. The hyperpolarization of pyruvate only lasts for a few minutes and this time is shortened when in the scanner due to excitation losses. The use of hyperpolarized pyruvate in the clinic is promising, but requires development of robust methods to ensure the reproducibility of results. The purpose of this work is to design an automated dynamic phantom system that will allow for the characterization and optimization of quantitative imaging

and analysis strategies. We have created a hydraulic pump system that reduces the variance in the reproducibility of hyperpolarized ^{13}C reaction rates and signal evolution. Eliminating error in the methods of injection, will allow focus on the reduction of error due to imaging strategies.

Table of Contents

Table of Figures

List of Tables

1 Hypothesis and Specific Aims

In a previous study a phantom had been constructed in order to investigate hyperpolarized pyruvate behavior in a biological environment. The design consisted of a single compartment containing an enzyme mixture into which the hyperpolarized pyruvate was injected. This phantom system is useful for strict control of all parameters such as the amount of pyruvate that reacts and maximizing SNR of the imaging sequence [1]. Despite the useful information gained from a simple phantom system, the differences between each injection leads to increased variability in phantom measurements. It must be ensured that the variability in the injections into the phantom system is minimized and the measurements being taken are as reproducible as possible. The error in the measurements obtained in the single compartment study mentioned above may be due to the variability in the rate of each injection. This error may be reduced by automating the injection process. **We hypothesize that a phantom and hydraulic pump system can be made that will improve the reproducibility of the injection rate, and therefore the hyperpolarized ^{13}C reaction rates.** The hypothesis was tested using the following specific aims:

1. **Design the phantom and syringe pump.**

The phantom was machined using ULTEM resin, which has a susceptibility close that of water and thus will minimize artifacts around the chamber interface. The phantom contains injection and exhaust ports that attach to a central chamber. The ports provide easy access for injection and simplify cleaning as the phantom can be flushed with water to remove any pyruvate or enzyme that may still be in the chamber. The phantom also contains a slot for urea, an important external reference that allows the resonant frequency of the system to be set accurately. It was also designed to accommodate a membrane that will be employed in future work to mimic tissue perfusion. The syringe pump was designed using all plastic materials. It has two syringes to hydraulically push the syringe containing the pyruvate.

2. **Test the reproducibility of the hydraulic syringe pump system outside of the MRI system.**

In order to ensure the accuracy of the injection rate, the hydraulic syringe pump was tested outside of the MRI environment using water rather than the hyperpolarized pyruvate. The injection rate tests included a test of the pump without the automatic injector system driving the system, a test of the automatic injector alone, and a test of the whole system combined with a long length to tubing to simulate the pump being distant from the injector system.

3. **Test the reproducibility of the hyperpolarized ^{13}C reaction rates in the phantom with and without the hydraulic pump.**

The reaction rates were tested by injecting a set amount of hyperpolarized pyruvate into the phantom and scanning it to obtain many spectra of the amount of pyruvate and lactate present as a function of time. The variability of the rates obtained from these spectra was compared across data sets.

2 Introduction and Background

2.1 Magnetic Resonance Imaging

Magnetic Resonance Imaging is a common diagnostic imaging modality that is used to provide excellent soft tissue contrast in the form of volumetric or spectroscopic data. This data is obtained without the use of ionizing radiation by manipulating the nuclear spin states of different materials within a given volume using a main static magnetic field, time-varying gradient fields, and short radiofrequency (RF) pulses. For the vast majority of clinical MRI systems, the magnetic field is created by a persistent superconducting electromagnet, and the RF pulses are generated by RF coils located inside of the scanner. Superconductivity is necessary to reach higher field strengths that provide a better signal to noise ratio. The RF coils are used to excite the spin system and detect the signals that they emit as they rotate within the static magnetic field. The gradient coils create magnetic fields which are superimposed, creating what are called the gradient fields that provide spatial encoding. There are also a set of shim coils that increase the homogeneity of the main magnetic field. ^{1}H nuclei, protons, are the nuclei predominantly viewed in MRI studies, but other nuclei can be interrogated using magnetic resonance as well. All of this equipment is used to manipulate the spins of nuclei in the patient.

2.1.1 Net Magnetization

A strong external magnetic field will cause the nuclei's spins to align either with or against the applied field. The alignment corresponds to two energy states, one high and one low, as seen in figure 2-1. At thermal equilibrium there is no difference in energy state if there is no significant magnetic field, but when an external magnetic field is applied, a population difference between the energy states arises.

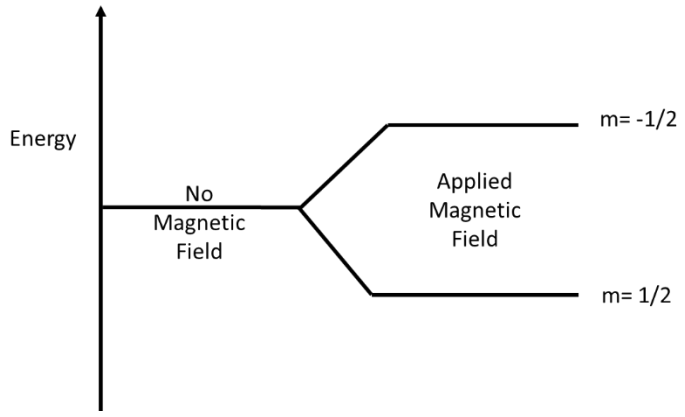

Figure 2-1 Energy diagram for a nucleus with spin number ½. The spins anti-parallel to the external magnetic field form the higher energy state.

Higher field strengths will increase the difference between these energy states and thus the difference in spin populations that contributes to a measurable net magnetization. This is the summation of the large number of parallel and antiparallel spins. For example, at 1T, the number of extra protons in the low energy state is about 3 protons per million. Since the number of protons typically sampled in one 2x2x5mm voxel of an image is about 10^{21} protons, assuming the density of water, the net magnetization is sufficiently strong that it can be detected using the MR detector coils. The spins not only align with or against the field, they also precess at a certain frequency. The frequency of this precession is related to the strength of the magnetic field and is defined by the Larmor equation (equation1):

$$\omega_0 = \gamma B_0 \qquad \text{Eq. 1}$$

where ω_0 is the angular (Larmor) frequency, γ is the gyromagnetic ratio, and B_0 is the superimposed static magnetic field. The Larmor frequency of hydrogen is 42.58 MHz/T.

2.1.2 Signal Excitation

Excitation angle, echo time, and repetition time determine contrast in gradient echo images. When an RF pulse at a certain excitation angle is applied, the net magnetization is tipped

into the transverse plane. The relationship between the excitation angle and transverse M_{xy} and longitudinal magnetization M_z is shown in figure 2-2.

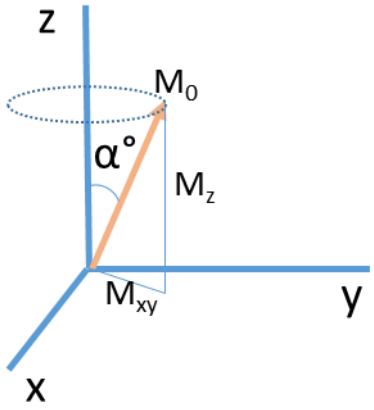

Figure 2-2 Relation of the flip angle, α, to M_{xy} and M_z. The flip angle is the angle between the net magnetization, M_0, and the z-axis.

After this excitation pulse, a signal in the form of a damped sinusoid called the free induction decay (FID) is obtained.

Once the net magnetization is in the transverse plane, the torque applied to the net magnetic moment by the static magnetic field causes constant rotation that can be detected by loop coils [2]. The received signal strength is dependent on the concentration of ^1H and the proximity to the detector and is also affected by the relaxation due to differences in the molecular environment.

2.1.3 Relaxation

The received signal is induced by the precession of the excited spins. Signal relaxation is characterized by tissue-dependent characteristics, spin-spin relaxation (T1) and spin-lattice (T2) relaxation time constants. T1, or spin-lattice relaxation, describes the return of longitudinal

magnetization (M_z) to equilibrium after RF (B_1) excitation. The effect of T1 relaxation on longitudinal magnetization is described by equation 2:

$$M_z(t) = M_0(1 - e^{-t/T1}) \qquad \text{Eq. 2}$$

where $M_z(t)$ is the longitudinal magnetization, t is the time after excitation and T1 is the time it takes for 63% of M_z to be recovered after a 90° RF pulse. When t=T1, the M_z magnetization will be $0.63M_0$. This illustrates the mechanism by which imaging sequences with a long repetition time (TR) between excitation pulses (TR>>T1) will allow full T1 relaxation. The longitudinal magnetization does not directly result in a signal, so a specific sequence must be used to determine T1. After the initial pulse sets M_z to 0 there is a delay and a second 90° pulse transforms the recovered M_z magnetization to M_{xy} and the resulting signal amplitude is recorded. By repeating this technique with differing delays, the points can be fit to an exponential equation to find T1[3]. The fit can be seen along with a diagram of the recovery in figure 2-3.

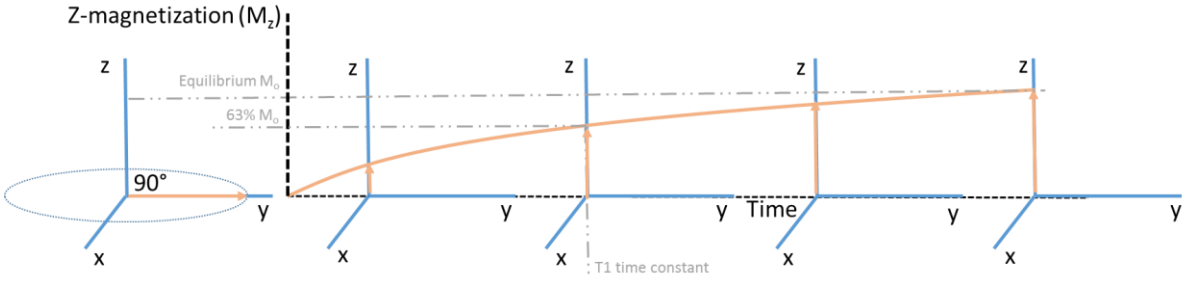

Figure 2-3 Exponential T1 recovery curve diagram. Initially the magnetization starts with $M_z(t<0)=M_0$, then after a 90-degree excitation magnetization is transferred into transverse plane ($M_{xy}=M_0$, $M_z=0$) and M_z recovers according to Eq 2.

The T2 relaxation, or T2 decay, is the result of intrinsic magnetic inhomogeneities and can be observed after any excitation pulse. The decay is caused by a loss of M_{xy} phase consistency due to local, or internal, magnetic field inhomogeneities. This loss in consistency is characterized as an

exponential decay where the time to decay to 37% of the peak signal is called the T2 relaxation time (figure 2-4).

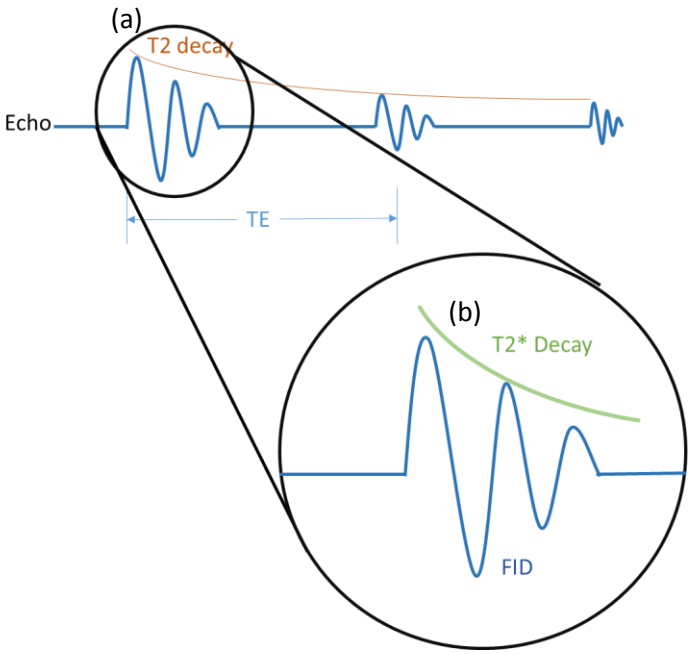

Figure 2-4 (a) T2 Decay: This is the result of intrinsic magnetic inhomogeneities that cause each successive FID to have a decreased amplitude relative to the previous FID. (b) T2* Decay: This is the result of inhomogeneities extrinsic to the subject that cause each FID to decay exponentially.

T2 relaxation is characterized in equation 3:

$$M_{xy}(t) = M_0 e^{-t/T2} \qquad \text{Eq. 3}$$

where $M_{xy}(t)$ is the transverse magnetization and t is the time after excitation at which it is observed. In equation 3, the sample is fully relaxed, where $M_z=M_{0,}$ prior to applying a 90° excitation angle. If not the sample is not fully relaxed, there is a sin(α) dependence on the excitation angle. When t=T2, M_{xy} will be equal to $0.37M_0$. Fluids typically have long T2 values, while tissues that are composed of heterogeneous molecular and structural environments have

shorter T2 values. T1 relaxation generally takes about 5 to 10 times longer than T2 relaxation and tissues with longer T1's usually also have longer T2's[2, 3].

Extrinsic magnetic field inhomogeneities can accelerate this spin-spin relaxation and further reduce T2. Because of these inhomogeneities, gradient echo sequences suffer from loss of signal and susceptibility artifacts are more prominent on gradient eco sequences than on spin echo sequences. These imperfections also include spatial variation in the magnetic field, and can be induced by contrast agents. In this situation, the decay constant T2 is reduced even more and referred to as T2* (figure 2-4).

2.1.4 Pulse Sequences

Forming multi-dimensional images from these signals requires repetition of a pulse sequence that excites the spin system and encodes the signal to k-space. Overall image contrast will depend on the time of repetition (TR) of the excitation pulse and the time of echo (TE), which is the time between excitation and signal measurement. During the TR, T1 recovery and T2 decay are both occurring. The choice of TE and TR will dictate which of these two processes will result in the dominant form of image contrast.

2.1.4.1 Pulse-Acquire Spectroscopy

MR spectroscopy is performed by using pulse sequences to evaluate shifts in frequency relative to a reference standard. These shifts are caused by different chemical shielding of MRI-visible nuclei within the molecular environment and can be used to determine the amount of a metabolite in the sample. A simple pulse-acquire sequence can be used to determine the relative concentration of spins contributing to unique spectral signatures. After the data is acquired, a Fourier transform is used to separate out the individual frequencies and they can be plotted as a spectrum. While water suppression can be added to this sequence to look for much more diluted metabolites, it often provides low signal-to-noise ratio (SNR) because they are typically much

less concentrated than water in tissue. Also, another disadvantage to pulse-acquire MRS is that there is no spatial encoding. Basic chemical shift imaging (CSI) can be used to localize signal to 1 cm^3 voxels which are achieved with the use of imaging gradients but at a cost of additional repetitions and much longer scan times. A post-processing technique that color codes the intensity of each metabolite inside of the voxels based on their concentration can be used after CSI to enhance visualization. This intensity map can then be placed on the corresponding anatomical image [2, 8].

2.1.4.2 Spin Echo Sequences

A spin echo is the result of two consecutive RF pulses rather than a single pulse that will only generate a FID. The spin echo sequence is one of the most commonly used pulse sequences and can provide T1, T2, and proton density weighting. This signal is induced with a 90° pulse, and a 180° RF refocusing pulse. The 180° pulse is set to occur at TE/2 to refocus the spin dispersion so that the echo forms at time TE [2]. When the pulse is applied, the spins refocus into a net transverse magnetization. Since initially they were becoming unaligned, after they are flipped their motion is maintained and they gradually align again. Multiple 180° pulses can be applied during a single TR to obtain several signals from one excitation. The amplitude of these signals decreases over time due to T2 decay [2, 6].

Equation 4 describes the amount of signal obtained with a spin echo pulse sequence.

$$S \propto \rho_H[1 - e^{TR/T1}]e^{-TE/T2} \qquad \text{Eq. 4}$$

where ρ_H is the signal producing proton density of the tissue, T1 and T2 are determined by the tissue, and TR and TE are set specifically to obtain the desired T1-weighted or T2-weighted image contrast. The signal obtained from moving protons, such as those in the blood, is not accounted for in this equation. An example of a spin echo pulse sequence can be seen in figure 2-5.

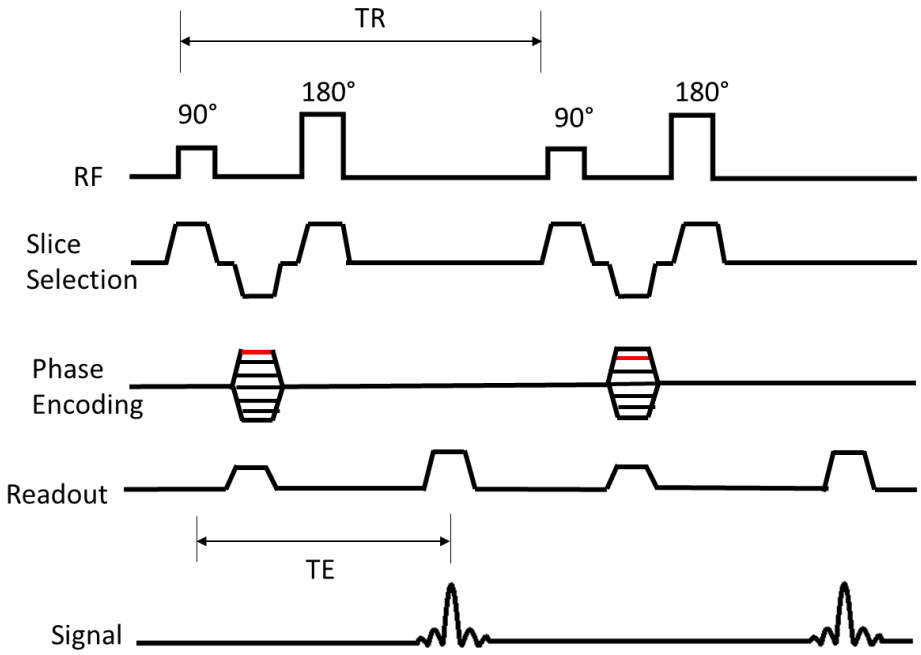

Figure 2-5 Spin echo pulse sequence diagram: The 90° pulse rotates bulk magnetization into the transverse plane and the 180° pulse refocuses them. The phase encoding gradient steps through different amplitudes to select spins of differing phases on each read out. The echo occurs at time TE.

Specific repetition times (TR) and echo times (TE) can impart image contrast that emphasizes one characteristic of the tissue while minimizing effects from the others. For example, T1 weighting emphasizes the differences between T1 characteristics of tissues. To obtain T1-weighted images from a spin echo sequence, a short TR and a TE are used. This combination will provide a large difference in the longitudinal recovery between tissues and minimize T2 contrast during signal acquisition. Because of this, tissues with a long T1 will appear to have low intensity and those with a short T1 will appear bright. T2-weighted sequences utilized long TRs and TEs. T2-weighted images generally display more tissue contrast than any other weighting, but also result in less transverse magnetization than T1-weighted images. Proton density weighting is obtained using a long TR and short TE to minimize T1 and T2 contrast[2, 7].

2.1.4.3 Gradient Echo Sequences

Gradient Echo sequences rely on gradients to control echo formation. A readout gradient with negative amplitude is applied to dephase the spins and then a gradient field of positive amplitude is used to rephase the spins, form the echo, and obtain the signal. A time delay may be used between the opposing gradients to control the timing of the echo. The gradient dephases and then rephases the spins. However, it cannot correct for dephasing due to local magnetic field inhomogeneities like the 180° focusing pulse of a spin echo sequence. This sequence simply dephases and rephases the free induction decay. A gradient echo sequence is depicted in figure 2-6.

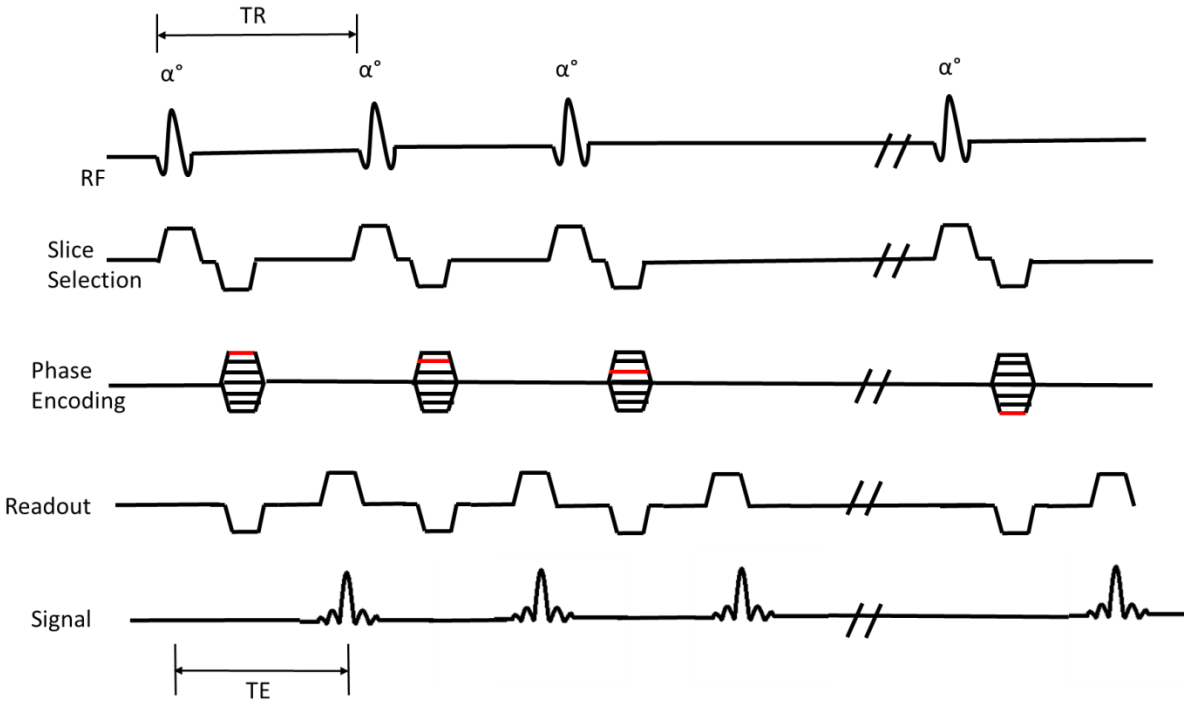

Figure 2-6 Simplified gradient echo pulse sequence diagram: TR is very short as is TE. The negative readout gradient dephases spins and the positive lobe rephases them. The applied flip angle is usually less than 90°.

Transverse relaxation is described by T2* which is much shorter than the relaxation described by T2. Because T2* is shorter than T2, variations in the external magnetic field are not canceled and the T2*-weighted images are affected by inhomogeneities in the main field and differences in magnetic susceptibility at tissue boundaries.

When the sequence has a short TR (<200ms), smaller flip angles create more steady-state transverse magnetization than larger flip angles [8]. There is always T1 and T2* weighting in an image, but each can be emphasized as desired. For example, with long TR sequences (>200ms), if the flip angle is less than 45° the image will be T2*-weighted. T1 weighting depends on the magnetic field strength and can also be emphasized under these conditions if a short TE is applied. An incoherent, or spoiled, gradient-echo sequence is used when T1 contrast is desired, but a very short TR is used. Spoiling gradients are applied which dephase the transverse magnetizations after every repetition.

2.1.5 Image Formation

During each pulse sequence the frequency-encoding gradient is used to encode the location of the protons in one direction, and a phase-encoding gradient localizes signals in the orthogonal dimension. These signals are encoded in the spatial frequency domain, otherwise known as k-space. The inverse Fourier Transform must be performed on k-space data to form images. These MR images can then be interpreted, providing a powerful, noninvasive diagnostic tool. Since the first good quality image of the wrist taken in 1977 and the first human head image in 1978, there has been a large interest in the applications of MRI [4, 5].

2.1.6 Phantoms

Phantoms are structures commonly used to ensure the reproducibility and quality of the data obtained during medical imaging procedures. They generally contain test objects specific to common problems and important aspects of the imaging modality in question. Simple phantoms

designed to test clinical MRI scanners are generally spheres containing a mixture of water and a paramagnetic salt to ensure reduced relaxation times and simulate the characteristics of the human body[9]. There are many different types of MRI phantoms including the ACR phantom and various phantoms that resemble the body to perform coil tests.

The ACR phantom is a cylindrical plastic phantom that is 16.5cm long and has a 20.4cm diameter. It contains a solution of 10mM nickel chloride and 45mmol sodium chloride. This mixture simulates biological conductivity. The phantom is typically placed in the head coil to evaluate system performance and reference lines are provided to help with alignment. Many tests can be performed using the ACR Phantom including spatial resolution, geometric distortion, image uniformity, low contrast detectability, slice thickness, slice position, and ghosting. Spatial resolution is tested using three small grid patterns with decreasing hole diameters of 1.1mm, 1.0mm, and 0.9mm. This test must be performed in two directions to evaluate the resolution of the frequency and phase directions. The passing criterion is stated as visualization of at least the 1.0mm grid in both directions. Geometric distortion is tested by measuring the dimensions of the phantom in the image and comparing them to the actual dimensions of the phantom. The limit for this test is that the image can only be up to ±2mm different from the actual measurements. The image uniformity is determined in the uniform section of the phantom. The signal in the brightest and darkest areas are measured, then subtracted and divided by the mean signal. From this, the peak-to-peak variation is determined as a percentage. The limit for this variation is 87.5% or greater for systems of 1.5T and below and 82% or greater for 3T systems. Low contrast detectability is tested using many slices where spokes made of decreasing diameter circular indentations that gradually become shallower and thus have less contrast with respect to the background of the phantom. The limiting number of spokes that should be seen is nine spokes for 1.5T or less[10].

MR scanners typically have a large number of associated RF coils that must be tested to ensure that the coils are operating properly. Coil testing requires a phantom that simulate the body part they are used for. For this reason, coil manufacturers provide homogenous phantoms filled with solutions that mimic biological conductivity.

From the phantoms discussed here, it is clear that reproducibility is an important aspect to implementing a QC program using a phantom to ensure reproducibility over time. This is also true for the testing of hyperpolarized pyruvate injections. While ^{13}C static phantoms provide a way of evaluating standard image quality metrics, such as spatial resolution, low contrast resolution, or artifacts, they do not provide information about the reaction that takes place in the human body. Dynamic phantoms provide information, such as reaction rates and reactant/product concentrations that offers insight into disease that could not previously be obtained through MRI. The human body is a dynamic system. Therefore, a dynamic phantom will more accurately describe what takes place in the presence of ^{13}C. A system that will reproducibly replicate reactions is needed to be able to reliably obtain information about measurement procedures. A single cavity model has been developed to provide a controllable reaction. This system is useful for strict control of all parameters and maximizing SNR[1]. Despite the useful information gained by a simple system, there was a coefficient of variation related to the study's data that could be reduced. Rapid manual injection of hyperpolarized pyruvate was identified as a potential source of variation in the system [1]. It is prudent to begin reducing the variation in the system to optimize new imaging methods moving forward. This study eliminates the variable introduced by hand injection and provides a way to ensure reproducibility in future studies.

2.2 Hyperpolarized Pyruvate

As stated in the Warburg effect, some tumor cells produce lactate even when in the presence of oxygen. It is thought that this occurs because tumor cells need to convert pyruvate to lactate at a high rate to create new biomass and proliferate. Although the Warburg effect (aerobic

glycolysis) is not an efficient way to produce ATP, most tumors have characteristic up-regulation of glucose transport and glycolytic enzymes, including lactate dehydrogenase. This method of making ATP does not provide as much as other methods, but it is a rapid way to provide the cell with energy[11]. Lactate dehydrogenase A facilitates the conversion of pyruvate to lactate and restores NADH to NAD^+. This restoration allows the continuation of aerobic glycolysis [12-14]. The conversion can be seen in figure 2-7.

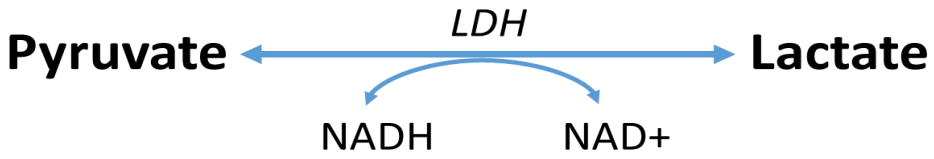

Figure 2-7 Pyruvate-Lactate conversion. Pyruvate converting into lactate restores NADH to NAD^+.

Tumors deprived of oxygen need a higher rate of glycolysis and are often more aggressive than tumors with a low glycolysis rate[15]. The central role of pyruvate in metabolism and the Warburg effect, its preexistence in vivo, the relatively high polarization values for hyperpolarized [1-^{13}C]-pyruvate, and its relatively long T_1 make it a promising metabolic contrast agent to visualize through MR imaging.

Hyperpolarization is a way to increase the signal-to-noise ratio for MR images. SNR is proportional to the nuclear spin polarization factor at thermal equilibrium. This factor is the fraction of spin alignment with an applied B_0-field and is defined in equation 5[16]:

$$P \approx \gamma \hbar B_0 / 2kT \qquad \text{Eq. 5}$$

where γ is the gyromagnetic ratio, $\hbar$ is Planck's constant divided by 2π, k is Boltzmann's constant, and T is the absolute temperature. At clinical field strengths thermal polarization is sufficient for protons due to their natural abundance. ^{13}C has a very low natural abundance and

very low relative signal compared to ^{1}H, At low temperatures the polarization factor for ^{13}C may be high enough to give an acceptable SNR, but in vivo temperatures are not favorable[16]. Because of this, high field strengths (B_0) are applied to compensate. Even with this increase in field, the polarization factor for ^{1}H at 3T is $1x10^{-5}$ and for ^{13}C is $2.5x10^{-6}$[17]. Hyperpolarization allows this polarization factor to be increased prior to the experiment to increase the SNR artificially. This increase is 10^4-fold compared to thermal equilibrium for certain substances such as [1-^{13}C]-pyruvate [18].

2.2.1 Dynamic Nuclear Polarization

Dynamic nuclear polarization (DNP) is a process in which the highly polarized spin state of electrons is transferred to nearby nuclei. This technique has been used to increase signal in MR images and visualize substances that were previously not able to be examined by means of MRI[19]. To induce DNP, the substance is mixed with a paramagnetic source containing free electrons and frozen to approximately 1K. The substance is placed in a high magnetic field and irradiated with microwave radiation. This radiation is applied at the energy required to transfer spin polarization from electrons to coupled atomic nuclei. After solid-state nuclear polarization reaches a plateau, the substance is ready to be used. The resulting polarized substance is thawed rapidly with a very hot solvent. Even though the absolute temperature of the solution is altered, polarization is retained. This mixture can be injected and scanned[16]. The improvement in SNR is a positive result of hyperpolarization, but it also has downsides. The polarization is not a renewable resource and is constantly being lost to different factors. The lifetime of ^{13}C ex vivo is typically 60 seconds, it's half-life is between 10-30 seconds, and it's T1 is 42 seconds at 9.4T[20, 21]. Spin-lattice relaxation is one source of loss as is signal excitation and depletion of the pool of the substance as it is transformed into its products [22, 23]. When the signal curves are obtained, the pyruvate curve has a large amplitude initially. The curve decays quickly and the lactate curve increases. As the pyruvate is converted to lactate, the polarization state of the ^{13}C label is

preserved. The lactate curve increases until the decay of the hyperpolarization is greater than the rate of lactate production. These signal curves can be characterized semi-quantitatively by calculating the normalized lactate signal, nLac, or fitting the curves to a model to determine the exchange rate constant, k_{PL} [24, 25].

2.2.2 Pharmacokinetic Analysis

The reaction in which pyruvate is converted to lactate was modeled with enzyme kinetics to find the velocity of the conversion. These velocities are scaled by the ratio of hyperpolarized substance, denoted with an asterisk, to total substance. T1 excitation and signal excitation losses are also accounted for in equation 6 and 7.

$$\frac{dL^*}{dt} = -\left(\frac{1}{T_{1,Lac}} + \frac{V_{LP}}{L^*+L} + \frac{[1-\cos(\alpha)]}{TR}\right)L^* + V_{PL}\frac{P^*}{P^*+P} \qquad \text{Eq. 6}$$

$$\frac{dP^*}{dt} = V_{LP}\frac{L^*}{L^*+L} - \left(\frac{1}{T_{1,Pyr}} + \frac{V_{PL}}{P^*+P} + \frac{[1-\cos(\alpha)]}{TR}\right)P^* \qquad \text{Eq. 7}$$

Where V_{LP} and V_{PL} are the velocities of the reactions from lactate to pyruvate and from pyruvate to lactate respectively. P and L are the "invisible" concentrations of endogenous pyruvate and lactate and ^{13}C-enriched agents with spin population at thermal equilibrium. P* and L* are the concentrations of hyperpolarized pyruvate and lactate. TR is the relaxation time and α is the flip angle. This is a simple two compartment system, but there is a certain flux between pyruvate and lactate. This is defined by k_{PL} and k_{LP}. These are the rates at which pyruvate is converted to lactate, the forward reaction, and at which lactate is converted to pyruvate, the reverse reaction. The rate constants are defined in equations 8 and 9.

$$k_{PL} = V_{PL}/(P + P^*) \qquad \text{Eq. 8}$$

$$k_{LP} = V_{LP}/(L + L^*) \qquad \text{Eq. 9}$$

This forward reaction rate was used in our group's previous study to show the dependencies of k_{PL} on enzyme activity and pool size in phantoms and in vivo. The value had an error associated with it that this study aims to reduce [1].

2.3 MR Compatible Syringe Pump

An MR-compatible injection system is a tool that is commonly used in clinical practice. Manual injections are common sources of error due to changes in the rate, volume, and timing of injections. The introduction of an automated system could greatly reduce the error involved in the research setting as well. Unfortunately, translation is not as simple as obtaining a clinical injection system. The volumes of the pumps used in the clinic are much too large to be employed on mice or for preclinical hyperpolarized imaging phantoms. Previous solutions to this problem have been successfully developed by other research groups [26-28]. One study developed a pump made of two 3ml syringes driven by two 10 ml syringes on an automatic injector. The plungers of the hydraulic drive syringes were opposing and attached to a sliding carriage. The injection syringe sat next to one of the drive syringes and its plunger was also connected to the sliding carriage. There was a check valve on the end of the injection syringe that had a receptacle for the hyperpolarized pyruvate and the injection line attached. The check valve allowed rapid withdraw and injection. The maximum delivery volume of this system was 2.4mL and the standard deviation was 0.7% for a range of volumes from 0.6-2.4ml[28]. This pump was designed to meet the needs of many of the same issues as the syringe pump. The main improvement that was desired in this study was a more compact design that can fit easily into the bore of the scanner to reduce dead volume and would use fewer syringes and less tubing. The design of the first pump [28] utilized two automatic injectors to inject and refill. Reducing the number of auto injectors will simplify the overall design, save space, and reduce variability between machines[28].

2.4 Motivation

There are several potential benefits to the development of such a syringe pump-phantom system. The first benefit is clinical translation. Being able to more accurately explain the reaction of hyperpolarized pyruvate in the body will help validate the imaging sequences being used in hyperpolarized studies because providing results with fewer sources of variation will allow the sequences to be investigated without outside errors.

There are also benefits to developing an MR-compatible syringe pump by itself. The pump will provide more precise injection rates that will improve the time-resolved signal obtained by the metabolism of hyperpolarized pyruvate. Also the system will be more accurate and represent more clearly the kinetic rate constants of the reactions that take place in vivo. These potential benefits motivated this study, which provided a MR compatible syringe pump and perfusion phantom system to reduce the variability inherent in manual methods.

3 Design of a Dynamic Hyperpolarized Phantom System

3.1 Design of a Dynamic Hyperpolarized Phantom System: Methods

The hydraulic syringe pump was designed to be used with an automatic injector system to drive it. The pump was created using non-ferromagnetic materials such as polyethylene plates and polyurethane screws and bars. A dynamic phantom was designed with features including a slot for urea and compatibility with a porous membrane for future perfusion experiments.

3.1.1 Sub Aim 1.1 Syringe Pump

The pump consists of one BD syringe suspended over another. The two are oriented in opposing directions. The top syringe is the injection syringe and the bottom syringe is the hydraulic actuator. The bodies of the syringes are connected by a sliding carriage and the plungers are secured by plates on either end of the device that can be tightened or loosened for removal. The bottom syringe is connected via a LuerLock fitting and 7 feet of PEEK tubing to a syringe on the automatic injector to drive the system. When the automatic injector is set to draw, the fluid in the bottom syringe will be pulled out, causing its body to move as if it were injecting. The motion of the bottom syringe injecting moves the top syringe in the opposing direction to draw. When the auto injector injects, the fluid is pushed into the bottom syringe pushing its body forward as if its plunger were being pulled back to draw. This motion causes the top syringe to move in the opposing direction and inject. The top syringe has a check valve attached to it that allows the syringe to draw hyperpolarized substrates from a receptacle that is fed from the hyperpolarizer and to inject the material into the phantom through PEEK tubing. The receptacle consists of a 20mL syringe that has been cut to the 5mL mark. The plunger of the syringe is cut flush with the rubber seal. A hole was drilled through the plastic and rubber for the tubing carrying the hyperpolarized pyruvate to go through. Finally, four small holes for relieving pressure were placed near the top of the syringe but below the rubber seal. The tubing is held in the receptacle through a hole in the sealed end of the plunger. The hyperpolarizer deposits the

hyperpolarized pyruvate into the receptacle allowing the syringe to draw it in through the use of the automatic injector. Once the desired amount has been drawn the pyruvate was injected into the phantom using the force of the automatic injector. The dimensions of the pump were specified to be 16.5cmX3.5cmX4.0cm. The length of the carriage for both syringes to extend and retract completely. The depth of the carriage allows the check valve to pass through the slot freely. The height provides for a 1cm spacing between the two syringes and accommodate the plates that hold the plungers. The pump and receptacle designs can be seen in figure 3-1.

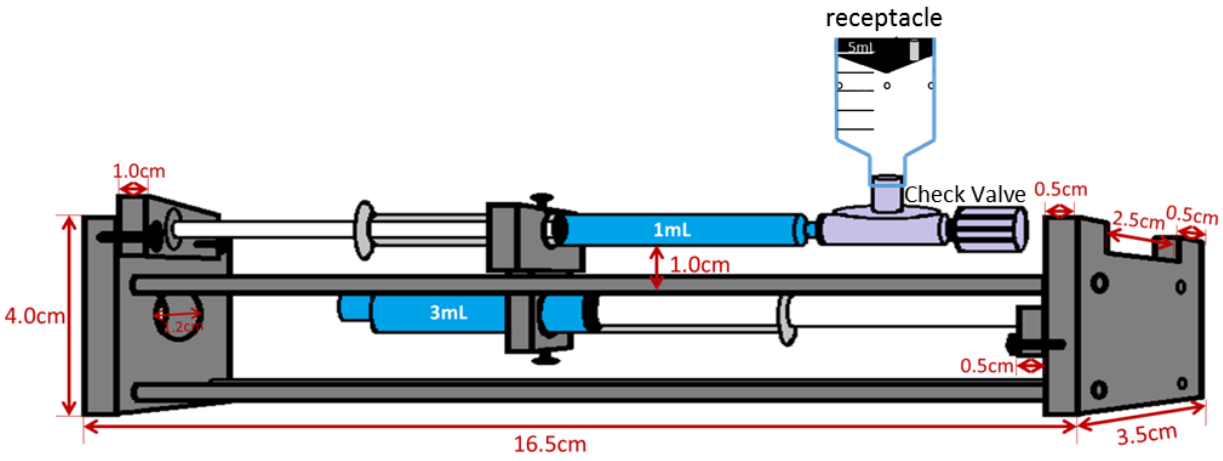

Figure 3-1 Hydraulic syringe pump and receptacle original design

The final pump design can be seen along with the finished receptacle attached in figure 3-2.

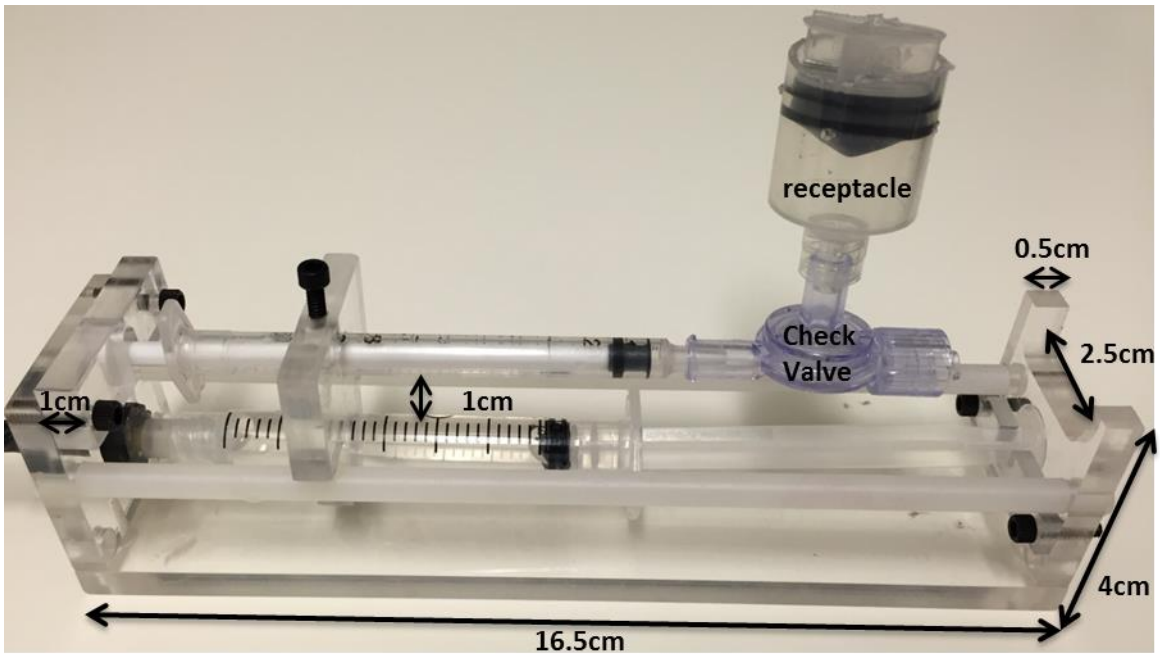

Figure 3-2 Finished syringe pump

3.1.2 Sub Aim 1.2 Phantoms

A prototype phantom was machined from a cylindrical piece of ULTEM. ULTEM is a high strength plastic material that has a magnetic susceptibility that is close to that of water, thus reducing artifacts at the edge of the interior phantom volume. This phantom was designed to include a reference urea chamber and a way to secure a perfusion membrane in future work. Urea is an important reference to have present while scanning. The reference is there to confirm that the correct frequency is set for imaging ^{13}C. Differing diameters and volumes were desired. The small chamber is to be used to determine the resolution of imaging sequences and the 1mL chamber is to be used to evaluate kinetic measurements. Finally, to perform future work with perfusion membranes, there must be an adequate way to secure the membrane between two chambers. The phantom consists of three sections, an outer cap with an intake port containing

threading to accommodate a LuerLock fitting to attach PEEK tubing to, a middle portion that consists of a 1mm diameter cavity, and an outer cap with an exhaust port threaded to fit a LuerLock fitting to attach PEEK tubing to. Both ports on the outer caps are surrounded by an inner rubber seal to ensure a watertight system. The three sections are held together by two screws on each end. The center section of the phantom is also designed with a cavity to fill with urea and seal closed with an ULTEM plug. The dimensions of the phantom can be seen in Figure 3-3.

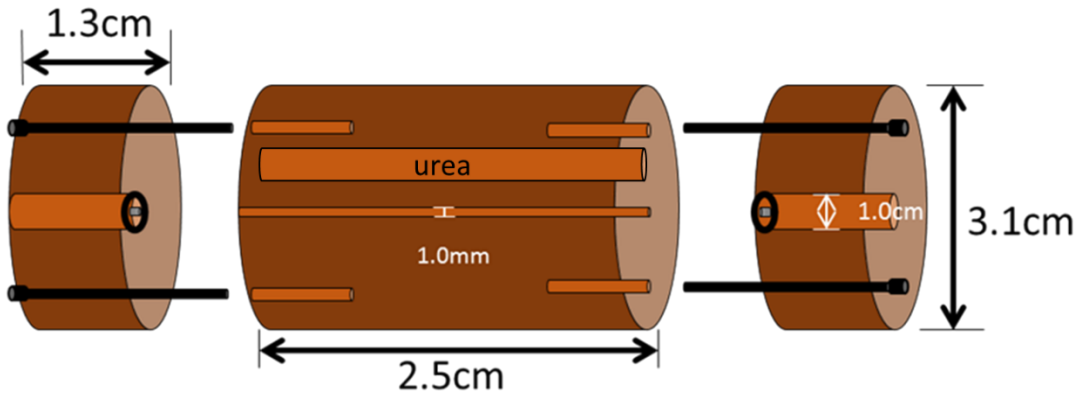

Figure 3-3 Prototype phantom original design with specifications

The finished prototype phantom can be seen in figure 3-4.

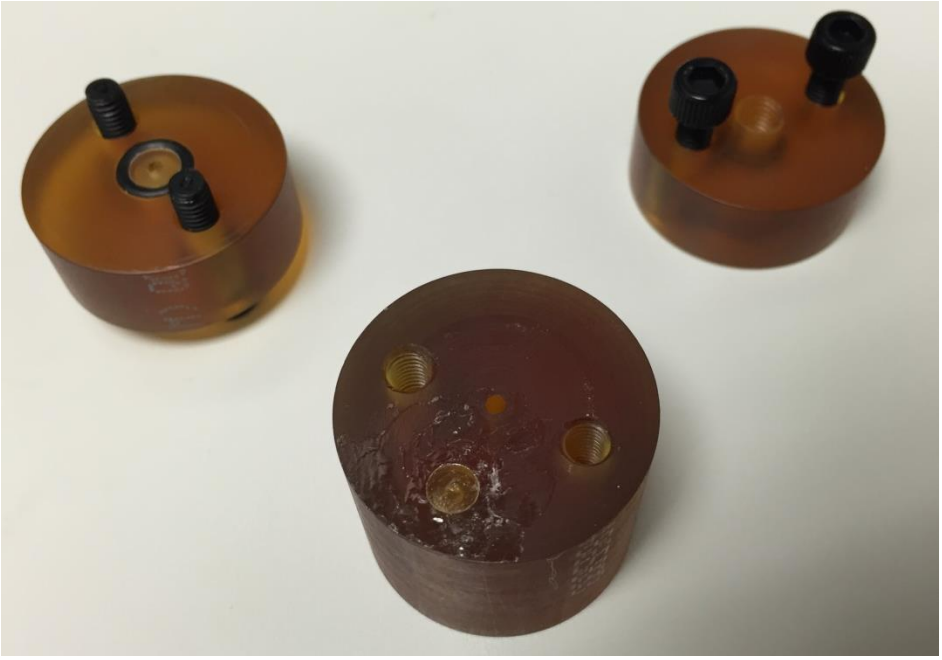

Figure 3-4 Finished prototype phantom

The T1 of the urea used throughout the experiment was tested in the cavity in this phantom. The phantom was scanned using a localizer to confirm positioning. Next, a saturation-recovery single-pulse acquisition with TR=2 seconds, 5kHz bandwidth, 2048 spectral points, and a 20° flip angle was used to determine the properties of the urea. The data was fit to Equation 2 (with t=TR) to find T1 using Matlab 2015b. The T1 was determined to be 0.782 seconds with a standard deviation of 0.0774 seconds. The graphical representation of the results is shown in figure 3-5.

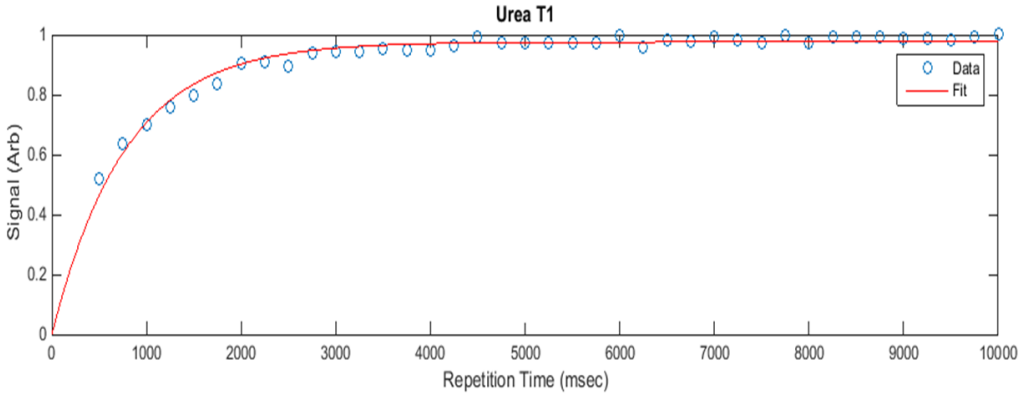

Figure 3-5 Saturation-recovery curve for ^{13}C-Urea

This is a very short T1 for urea. The typical T1 for urea is on the order of 20 seconds [28]. The shortened T1 in this case is due to the heavy gadolinium doping. The concentration in the mixture is 8M urea doped with 1.98mM Magnevist.

Semi-permeable membranes were initially considered for use in the phantom but it was determined that the rate of flux across the membrane was not high enough to be compatible with the very short observable lifetime of hyperpolarized substrates. The membrane that was ultimately used was a porous membrane constructed from Small Parts Plastic Shim stock with the color code “coral” and a thickness of 0.0127mm that had been punctured with a laser.

The shim stock was initially scanned to ensure that it would not create new artifacts within the dynamic hyperpolarized phantom. It was placed in a plastic vial filled with water. The resulting proton images can be seen in figure 3-6.

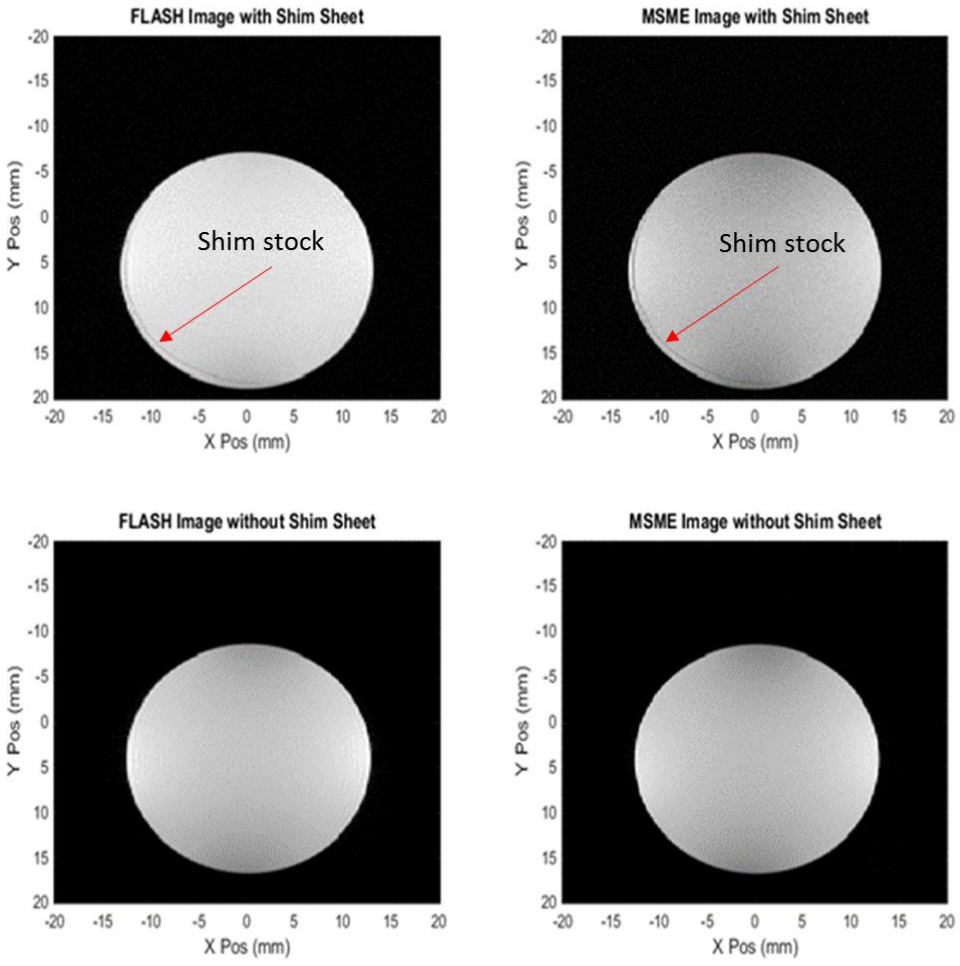

Figure 3-6 FLASH and MSME proton images with and without shim stock

There are no artifacts seen on the FLASH images which suggests that the susceptibility of the material is close enough to water that it would not generate artifacts or broaden spectral peaks in future experiments.

Pores for the shim stock membrane were created in house with a ProMaster Optec laser. The membrane was 0.0127mm thick and constructed with a pore size of 50 microns with 200 micron spacing between pores. The pore size selected was the minimum pore size for the specified thickness and was based on the capability of the laser. A design including many holes close together was chosen to ensure an even concentration of the fluid flowing out of the surface of the membrane. These pores allowed enough flow to quickly fill the cavity of the prototype phantom with little pressure. From these results it was concluded that this would be a feasible approach to creating a perfusion membrane. The final product was made to these specifications and can be seen in figures 3-7 and 3-8.

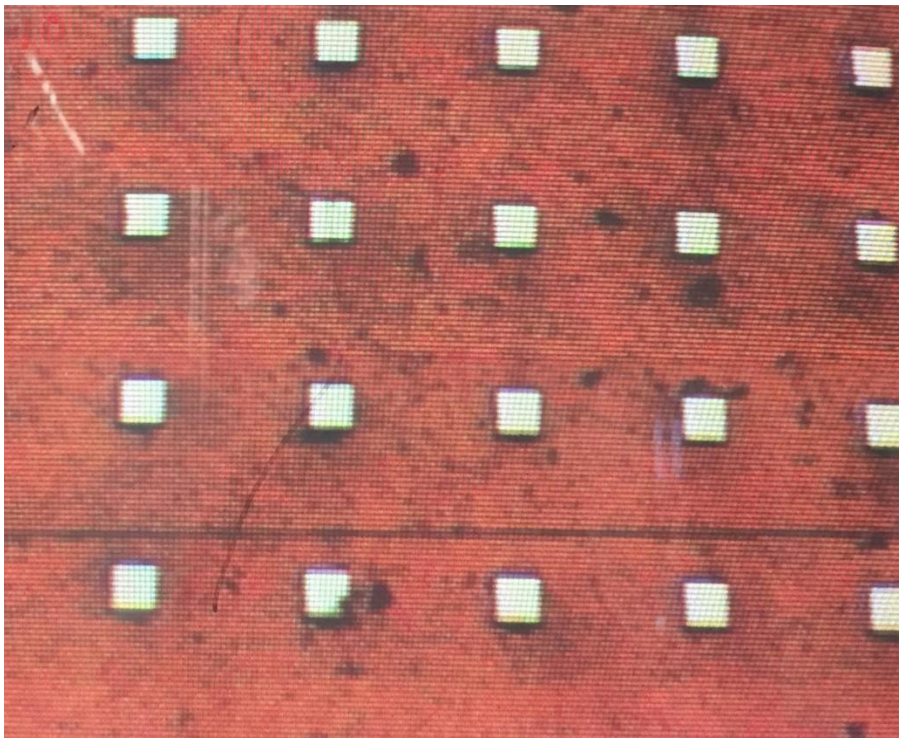

Figure 3-7 Magnified shim stock membrane

Figure 3-8 Porous area of shim stock: The entire sheet was cut to have dimensions of 3x2cm. The box drawn on the sheet indicates the perimeter of the porous area, ensuring proper placement in the phantom.

The reaction phantom was designed to favor the use of the shim stock membrane based on feasibility as demonstrated above. The phantom was machined from a cylindrical piece of ULTEM. The cylinder was 4cm long and 3.1cm in diameter. A coronal cut was made in the center of the phantom and a cavity was constructed with specific dimensions. The top section of the cavity was machined to be 2cm long by 1cm wide by 0.1cm deep to give a top cavity volume of 200 microliters. The bottom cavity was machined to be 2cm long by 1cm wide by 0.5cm deep to give a bottom cavity volume of 1mL. All dimensions can be seen in figure 3-9.

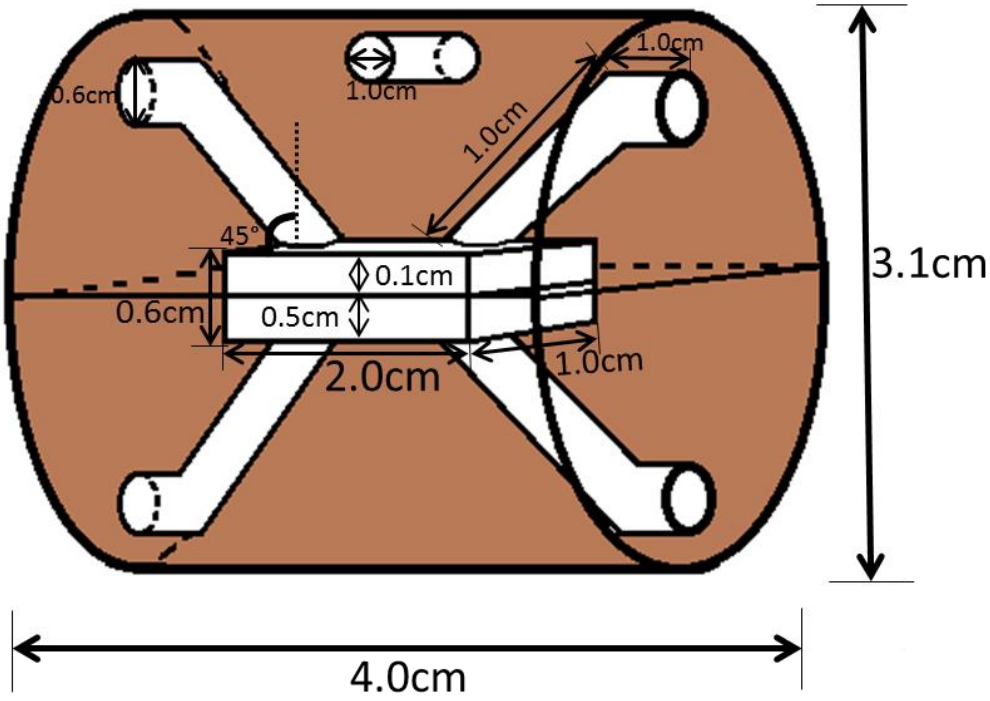

Figure 3-9 Reaction phantom original design

The bottom cavity was surrounded by an O-ring to hold the membrane in place. Both the bottom and top section of the cavity have an input and exhaust port, making four ports in total, coming off of the cavity at a 45° angle so that the openings of the ports into the cavity are easy to access in the scanner. The ports each turn to come out of an end of the phantom as threaded holes. The threads match LuerLock fittings that attach to PEEK tubing. The bottom cavity holds the enzyme and coenzyme while the upper cavity is where the pyruvate flows through. The resulting structure is shown in figures 3-10 and 3-11.

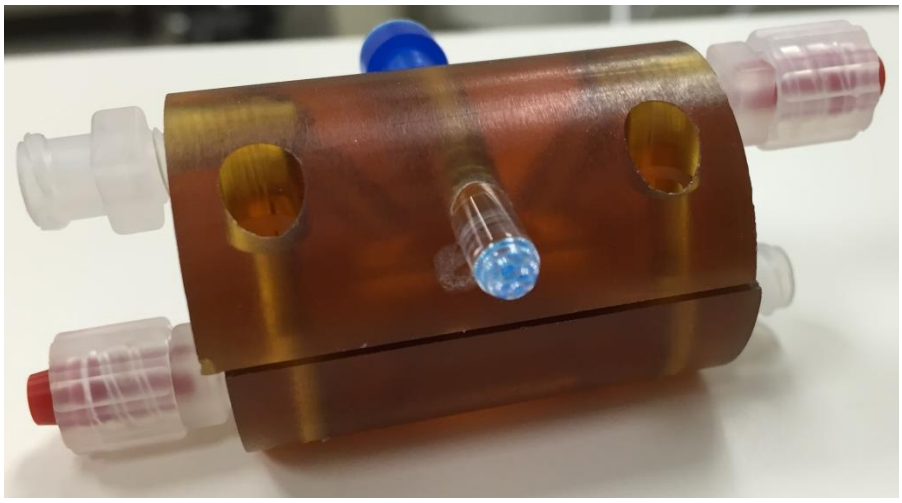

Figure 3-10 Finished reaction phantom

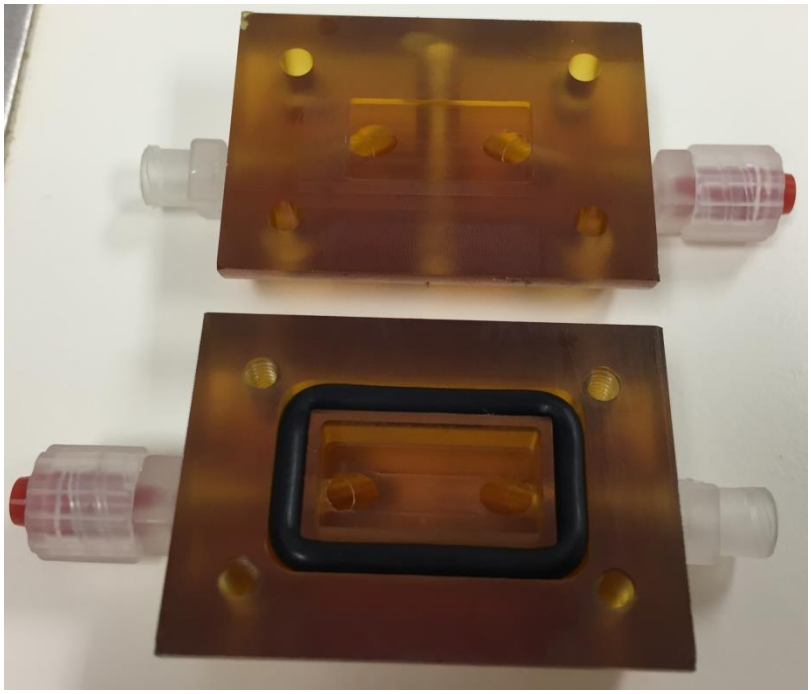

Figure 3-11 Finished reaction phantom cavities

The urea bulb was constructed from a 5mm glass NMR tube that was cut to 4 cm in length, filled with the urea investigated above and then plugged on the open end with an NMR cap.

4 Hydraulic Syringe Pump Reproducibility

4.1 Hydraulic Syringe Pump Reproducibility: Methods

The finished syringe pump was initially tested outside of the magnet initially to ensure functionality before testing with hyperpolarized substances. A relative amount of accuracy was established between the manual, automatic and automatic but remote injections. A set of measurements was taken by driving the syringe pump with an external syringe by hand. The pump was refilled completely and 0.2mL of water was injected. Using the density of water, 1g/mL, the set amount of liquid injected into a weigh boat was weighed using a digital scale and converted to find the volume actually injected. Twenty data points were taken and the standard deviation and percentage error were calculated by comparing the volume to the target volume. The accuracy of the automatic injector system was also tested by injecting 0.2mL water into a collecting tray and weighing it. The same method was used to determine the injected volume. The automatic injector is shown in figure 4-1 below.

Figure 4-1 Automatic injector to drive hydraulic syringe pump

The variances of the two data sets were tested using an F-test and then these measurements were compared to the first set of measurements using a two-sample t-test to determine whether the means of the two data sets are equal.

The pump was also tested using 7ft of PEEK tubing with an inner diameter 0.125 cm connecting the external drive syringe on the automatic injector to the pump to simulate a remote connection between the injector and syringes. The target volume was 0.4mL. Data points were taken for this test and compared to the manually injected data and the standard deviation and percentage error were also calculated. This data was also compared to the manual injections using an F-test and a two sample t-test to determine whether the means of the two data sets are equal.

The dead volume of the syringe was determined by filling the syringe to 0.3mL with an empty check valve attached and then injecting the water onto a weigh plate to be measured. The

weight was converted to volume using the density of water and then the actual volume injected was subtracted from the volume that should have been injected. This difference is the result of the fluid having to fill the extra dead volume.

4.2 Hydraulic Syringe Pump Reproducibility: Results

4.2.1 Manual Pump vs. Automatic Injector Results

The receptacle was filled with water as mentioned above and data points were obtained by refilling and injecting a set amount. The mean absolute percentage error was calculated using equation 4-1.

$$MAE = \frac{1}{n}\sum_{i=1}^{n}|f_i - y_i| \times 100\% \qquad \text{Eq. 4-1}$$

The results of this test are shown in table 4-1.

Measured (mL)	Desired Amount (mL)	Absolute Value of Difference (mL)
0.195	0.2	0.005
0.192	0.2	0.008
0.194	0.2	0.006
0.199	0.2	0.001
0.196	0.2	0.004
0.198	0.2	0.002
0.197	0.2	0.003
0.202	0.2	0.002
0.206	0.2	0.006
0.203	0.2	0.003
0.199	0.2	0.001
0.191	0.2	0.009
0.187	0.2	0.013
0.196	0.2	0.004
0.195	0.2	0.005
0.197	0.2	0.003
0.192	0.2	0.008
0.196	0.2	0.004
0.187	0.2	0.013
0.193	0.2	0.007
Average of Measured	**Mean Absolute Error**	**STD of Measured Amount**
0.196mL	**0.54%**	**0.0048**

Table 4-1 Accuracy test results for hydraulic syringe pump driven by hand

The mean absolute error was found to be 0.54% and the standard deviation was 0.0048mL for the syringe pump when operating it by hand with a short amount of PEEK tubing.

A 1mL syringe was then filled with water and placed in the automatic injector. The auto injector was set to inject 0.2mL. The final error is a comparison between the amount of water measured on output and the amount that was programmed into the console. The mean absolute percentage error in this table is calculated the same way as above. The results can be seen in table 4-2.

Measured (mL)	**Desired Amount (mL)**	**Absolute Value of Difference (mL)**
0.2005	0.2	0.0005
0.2001	0.2	1E-04
0.2008	0.2	0.0008
0.2011	0.2	0.0011
0.2001	0.2	1E-04
0.2	0.2	0
0.2001	0.2	1E-04
0.2007	0.2	0.0007
0.1998	0.2	0.0002
0.201	0.2	0.001
AVG	**STD**	**Mean Absolute Error**
0.20042	0.000435	0.046%

Table 4-2 Accuracy results for the hydraulic syringe pump driven by automatic injector system

The automatic injector does not reach exactly 0.2mL every time on the console. This variance could be due to mechanical shortcomings in the stopping mechanism, discrete control of motors in the automatic injector and the small volumes that are being used in the experiment. The mean absolute percentage error of the measurements compared to the desired volume was 0.046%. This is an order of magnitude smaller than the error of the hydraulic syringe pump when driven by hand.

An F-test was performed using Microsoft Excel to determine whether the variances in the two data sets are equal. The null hypothesis was that the two tests have the same variability. The results are shown in table 4-3 below.

F-Test Two-Sample for Variances

	Manual Inject	***Automatic Injector***
Mean	0.196	0.2004
Variance	2.33E-05	2.11E-07
Observations	20	10
df	19	9
F	110.4	
P(F<=f) one-tail	2.11E-08	
F Critical one-tail	2.95	

Table 4-3 F-test for variance of manual injections and the automatic injector system

A significance level of $\alpha=0.05$ was assumed. Since the F statistic was found to be greater than the F Critical value, the two variances are not equal and a t-test assuming unequal variances should be used. A t-test with a null hypothesis that the means are equal was performed. This t-test assuming unequal variances was calculated using Microsoft Excel and the results are shown in table 4-4.

t-Test: Two-Sample Assuming Unequal Variances

	Manual Inject	*Automatic Injector*
Mean	0.196	0.2004
Variance	2.33E-05	2.11E-07
Observations	20	10
Hypothesized Mean Difference	0	
df	20	
t Stat	-4.29	
P(T<=t) one-tail	0.00018	
t Critical one-tail	1.73	
P(T<=t) two-tail	0.00036	
t Critical two-tail	2.09	

Table 4-4 Two-sample t-test assuming unequal variance: Determines if there is a difference in means between manual injections and the automatic injector.

A significance level of $\alpha=0.05$ was assumed and since the P two-tail value is less than 0.05, the null hypothesis should be rejected. There is a statistically significant difference between the means.

4.2.2 Manual Hydraulic Pump vs. Longer Line Hydraulic Pump Test

The bottom syringe of the hydraulic syringe pump was connected to the external syringe on the automatic injector via 7ft of PEEK tubing with an inner diameter of 0.125 cm. The receptacle was placed on the check valve and filled with water similar to how it would be in an actual experiment. The results were calculated the same way as the manual hydraulic pump results and are shown in table 4-5.

Measured (mL)	Desired Amount (mL)	Absolute Value of Difference (mL)
0.387	0.4	0.013
0.4	0.4	0
0.387	0.4	0.013
0.39	0.4	0.01
0.398	0.4	0.002
0.388	0.4	0.012
0.387	0.4	0.013
0.394	0.4	0.006
0.382	0.4	0.018
0.396	0.4	0.004
Average	**Mean Absolute Error**	**STD**
0.391	0.91%	0.0058

Table 4-5 Accuracy results for hydraulic syringe pump using 7ft driving line

The mean absolute percentage error was determined to be 0.91% and the standard deviation was 0.0058mL. To perform the following statistical tests, the measurements were scaled by ½ assuming that the error scales with the target volume. An F-test was performed using Microsoft Excel to determine whether the variances in the manual inject and long line pump system data sets are equal. The null hypothesis was that the two tests have the same variability. The results are shown in Table 4-6 below.

F-Test Two-Sample for Variances

	Manual Inject	*Long Line Pump System*
Mean	0.196	0.196
Variance	2.33E-05	8.41E-06
Observations	20	10
df	19	9
F	2.76	
P(F<=f) one-tail	0.061	
F Critical one-tail	2.95	

Table 4-6 F-test for variance of manual injections and the pump system with a long line

A significance level of $\alpha=0.05$ was assumed. Since the F statistic was found to be less than the F Critical value, the two variances are equal and a t-test assuming equal variances should be used. A t-test with a null hypothesis that the means are equal was performed. This t-test assuming equal variances was calculated using Microsoft Excel and the results can be seen in table 4-7.

t-Test: Two-Sample Assuming Equal Variances

	Manual Inject	*Long Line Pump System*
Mean	0.196	0.196
Variance	2.33E-05	8.41E-06
Observations	20	10
Pooled Variance	1.85E-05	
Hypothesized Mean Difference	0	
df	28	
t Stat	0.180	
P(T<=t) one-tail	0.429	
t Critical one-tail	1.70	
P(T<=t) two-tail	0.858	
t Critical two-tail	2.05	

Table 4-7 Two-sample t-test assuming unequal variance: Determines if there is a difference in means between manual injections and the pump system using a long drive line.

A significance level of α=0.05 was assumed and since the P two tail value is greater than 0.05, the null hypothesis cannot be rejected. There is no statistically significant difference between the means.

Because there is a statistically significant difference between the means of the manual injection data and the automatic injector, this means that adding the automatic injector to the system will change the variance of output of one of the mechanisms. Because the automatic injector is a system of know precision, the difference is likely due to the syringe pump being more variable than the automatic injector. There is no statistically significant difference between

the means of the manual injection and the long line pump system. This means that adding the long line to the system will not make the results differ much compared to the pump by itself with a shorter line.

4.2.3 Dead Volume Results

The syringe was filled with 0.3mL of water and the dry check valve was then secured on the end of the syringe. The 0.3 mL was then pushed from the syringe and the water that exited the system was weighted. Converting this measurement as discussed above and subtracting it from the 0.3mL determined what remained in the check valve. The results can be seen in table 4-8.

Draw	**Push**	**Difference (Dead Volume)**
0.3	0.21	0.09
0.3	0.24	0.06
0.3	0.18	0.13
0.3	0.23	0.07
0.3	0.22	0.08
0.3	0.23	0.07
	STD	**Mean Difference (Mean Dead Volume)**
	0.02	0.08

Table 4-8 Dead volume results

The dead volume that needs to be accounted for it only about 0.04, or half of this value. This is due to the way the syringe draws in the back half of the dead volume before drawing any liquid, leaving 0.04mL of dead volume before the fluid in the syringe and after the fluid. When the syringe injects, the half of the dead volume behind the fluid is trapped in the check valve and does not exit the system. Since there is a difference in the dead volume with every injection, as seen in table 4-8, using a mean value to fill that volume does reduce the error but does not

eliminate the error completely. The variability in dead volume will ultimately contribute to the total variability of the system.

5 Signal Curve Reproducibility Improvement

5.1 Signal Curve Reproducibility Improvement Methods

Tests were run to evaluate the reproducibility of the signal curves generated during a scan in which pyruvate is converted to lactate through the use of the enzymes LDH and NADH. The phantom shown in Figure 3-10 was used without the membrane in place. A batch of 5mL of the 50 U/mL LDH enzyme mixture was made to support 5 trials in one day from the same set of preparations to eliminate enzymatic activity as an experimental confounding factor. A unit is defined as the amount of LDH that it takes to catalyze 1µmol of pyruvate per minute at 30° C when NADH is in excess. 0.14mM NADH, and 0.038mM of Tris buffer with a pH of 7.6 were the concentrations in the final mixture. Each phantom setup contained 1.0mL of the enzyme mixture. Two sets of experiments were performed to compare the reproducibility of the two scenarios. First, we assessed the reproducibility of data obtained using hand injections. To perform this experiment, someone had to be present in the room at the time of the scan. The phantom was assembled in the scanner with 1mL of the enzyme mixture already present in the system. The hyperpolarized pyruvate flowed from the polarization system and into a receptacle on the wall. The pyruvate was drawn from the receptacle and injected as quickly as possible using 81 cm of peek tubing and a 3mL syringe. A second set of scans using the same parameters was taken using the hydraulic syringe pump and automatic injector to assess the reproducibility of data taken using this system. The receptacle for the hyperpolarized pyruvate was attached to the check valve on top of the pump. The MR compatible automatic injector module was placed just inside the door of the scan room and the console was place outside. The pump was placed on the sled connected to the same 81 cm of PEEK tubing used before. The 7ft of PEEK tubing was used to connect the syringe pump to the drive syringe in the automatic injector. No one was required to be in the scan room as the injector could be controlled by the console. The parameters specific to the syringe pump can be seen in table 5-1.

20mL Syringe to Drive	**Draw**	**Inject**
Rate	40mL/min	40mL/min
Duration	8.0sec	9.0sec
Volume	5.34 mL	6mL

Table 5-1 Automatic injector program parameters

It is important to note that the volume above is not the volume finally injected. It is the volume injected by the 20mL drive syringe to push 1mL of liquid from the injection syringe. The final volume of pyruvate injected was 0.86mL due to the dead volume mentioned above. The reason for the longer injection time is due to the vacuum that is created in the drive syringe during draw. The air gap that is created must be overcome before the fluid can be pushed and if extra time is not added the volume injected will be smaller than expected.

A 7T Biospec small animal MR system (Bruker Biospin MRI) was used to collect the data and the pyruvate was hyperpolarized using a HyperSense dissolution dynamic nuclear polarization system (Oxford Instruments). After placing the phantom at isocenter, a localizer was taken before each dynamic hyperpolarized ^{13}C scan. 0.86mL of pyruvate was injected into the phantom at the beginning of each scan. The scans were three minute pulse-acquire scans using a 20° flip angle, a TR of 2 seconds, a 2.5 kHz bandwidth, and 4098 spectral points. .

5.2 Signal Curve Reproducibility Improvement Results

5.2.1 Hand Injection Results

The resulting signal curves had a normalized lactate standard deviation of 0.034 and a coefficient of variation of 17.8%. The k_{PL}'s, standard deviation was 0.004 and the coefficient of variation was 23.1%. The complete set of results can be seen in table 5-2.

Hand Injections	Fitting (k_{PL})	Pyruvate Signal	Lactate Signal	Normalized Lactate
1	0.018	$2.30x10^7$	$5.44x10^6$	0.191
2	0.022	$1.13 x10^7$	$3.23x10^6$	0.222
3	0.014	$1.75 x10^7$	$3.20 x10^6$	0.155
Mean	0.018	$1.73 x10^7$	$3.95 x10^6$	0.189
STD	**0.004**	$5.87x10^6$	$1.29 x10^6$	**0.034**
Co-Var (%)	**23.1**	33.9	32.5	**17.8**

Table 5-2 Signal curve variance results for hand injections

5.2.2 Hydraulic Syringe Pump Injection Results

The phantom was assembled again without the membrane and the hydraulic syringe pump was connected to the inlet of the phantom via the same length of PEEK tubing used in the hand injections. Four data points were obtained with the hydraulic syringe pump. The standard deviation and coefficient of variation for the normalized lactate signal were 0.019 and 10.5%, respectively. For the fitting, or k_{PL}, the standard deviation and coefficient of variation were 0.002 and 14.7%, respectively. Table 5-3 contains the results for this trial.

Scan No	Fitting (k_{PL})	Pyruvate Signal	Lactate Signal	Normalized Lactate
1	0.012	$6.50x10^6$	$1.40\ x10^6$	0.177
2	0.012	$4.71\ x10^6$	$9.72\ x10^5$	0.171
3	0.012	$2.49\ x10^6$	$4.75\ x10^5$	0.160
4	0.015	$3.29\ x10^6$	$8.45\ x10^5$	0.204
Mean	0.013	$4.25\ x10^6$	$9.24\ x10^5$	0.178
STD	**0.002**	$1.76\ x10^6$	$3.82\ x10^5$	**0.019**
Co-Var (%)	**14.7**	41.4	41.4	**10.5**

Table 5-3 Signal curve variance results for hydraulic syringe pump injections

The coefficients of variation for normalized lactate and for k_{PL} were lower than both the previously mentioned hand injections and the published hand injection data.

5.2.3 Hydraulic Syringe Pump vs Hand Injection Discussion

The values stated above correspond to a 36% improvement in the coefficient of variation of pharmacokinetic analysis and a 41.1% improvement in the coefficient of variation of the normalized lactate signal compared to the hand injections done in this study. The percentage of improvement between all hand injection data and the pump injection data are shown in table 5-4.

% Improvement	Fitting (k_{PL})	nLac
Pump vs. Hand Injections	36.0%	41.1%
Pump vs. Previous Publication	22.4%	12.7%

Table 5-4 Comparison table for this study and previous publication

6 Discussion and Conclusions

A hydraulic syringe pump phantom system was designed that improved the reproducibility of measurements in comparison to those using manual injections. The injection pump was tested and the reproducibility of the reactions was shown to compare favorably to those initiated by manual injections. The syringe pump not only improves reproducibility, but it also eliminates the need for someone to be in the room to inject by hand when performing an experiment. A new phantom structure was designed and implemented that uses fewer reagents than previous ones. It contains a slot for a urea bulb to use as a reference to ensure that the correct frequency is used in the experiments. It is also compatible with semipermeable membranes for the future development of a perfusion phantom.

The research project presented here was on an accelerated timeline due to coursework and an early transition into a clinically-oriented DMP program. One limitation is due to the receptacle on the syringe pump. When pyruvate comes into the receptacle, the liquid sloshes inside of the container. If the pump is not perfectly upright and the modified plunger shifts due to the air in the container being displaced by the incoming pyruvate, the receptacle may leak. The results of the hand injections used in this study were larger standard deviations and coefficients of variation than previously reported [1]. There was a difference in the phantom structure and the volume, which may lower the SNR. In this study, that may be the cause of the difference in coefficients of variation and standard deviations. There was also a difference in the way the reagents were mixed that may have contributed to this difference. Some of this discrepancy may be due to having fewer replicates in this study than the other (N=3 vs N=7) [1].

There was not a sufficient amount of data to perform a statistical test, but the aim of this experiment was to improve on reproducibility with regards to the data from a previous paper and our own reproduction of that data. Considering that the coefficient of variation is an indicator of reproducibility, it has been used as the main method of comparison for these three methods.

The results of the hydraulic syringe pump test suggest that such a mechanism would be beneficial to have in a research setting. The hydraulic system reduced variation in the k_{PL} by 36% compared to manual injections in this study and by 22.4% in comparison to the results of the previous publication. It also reduced the variation in the normalized lactate signal by 41.1% and 12.7% compared to our control data and the coefficients of variation from the previous paper. These improvements are not isolated to this one study. In the future, the system could be used to improve the variation of all in vitro (phantom) and in vivo measurements involving hyperpolarized imaging agents. We believe that the results of this study prove that the system will help provide a reproducible way to test new imaging sequences and maximize reproducibility among measurements and comparisons in vivo.

6.1 Future Directions

Further developments could be made to enhance the dynamic hyperpolarized MRI phantom system that is described herein. The receptacle for the pyruvate on the top of the check valve could be made from a syringe with a larger diameter to better catch the pyruvate flowing in at a high velocity. Although a larger hole on the top of the modified plunger may prevent leaking and movement by releasing the pressure created by the incoming pyruvate more rapidly than the four needle punctures do. As of now, the maximum amount of fluid that can be injected is 0.86mL. Another version of the middle structure of the pump could be machined to allow larger syringe sizes to be used.

It could also be utilized for animal studies with the right modifications. In this case, where dead volume is a concern, the pump is able to sit inside the bore of the scanner, allowing for a reduction in catheter length and thus dead volume.

Simulations could be done to find appropriate pore sizes for a perfusion membrane that would allow for mixing, but not be so large as to allow free flow and displacement of enzymes.

The shim stock is a promising material and the phantom functions the way that it should when the membrane is present. Perfusion is an important biological characteristic and that can have significant impact on signal evolution in vivo, and thus affect the characteristics of dynamic hyperpolarized MRI sequences [1].

The results of this work will ultimately help to improve the reproducibility of dynamic hyperpolarized MRI phantoms, which will be a crucial component in the optimization and validation of imaging strategies for preclinical and clinical imaging research. In the future, the system will not only improve accuracy; it will also more accurately explain signal evolution in vivo. This system has the potential to make significant contributions to imaging research that may lead to a wide range of scientific breakthroughs.

7 Bibliography

1. Walker, C.M., Jaehyuk Lee, Marc S. Ramirez, Dawid Schellingerhout, Steven Millward, and James A. Bankson, A catalyzing phantom for reproducible dynamic conversion of hyperpolarized [1-(1)(3)C]-pyruvate. PLoS One, 2013. 8(8): p. e71274.

2. Bushberg, Jerrold T., The Essential Physics of Medical Imaging. 2011: Wolters Kluwer Health.

3. Elster, A.D. and J.H. Burdette, Questions & Answers in Magnetic Resonance Imaging. 2001: Mosby.

4. Qayyum, A., MR Spectroscopy of the Liver: Principles and Clinical Applications. RadioGraphics, 2009. 29(6): p. 1653-1664.

5. Bernstein, M.A., K.F. King, and X.J. Zhou, Handbook of MRI Pulse Sequences. 2004: Academic Press.

6. Haacke, E. Mark, Robert W. Brown, Michael R. Thompson, and Ramesh Venkatesan, Magnetic Resonance Imaging: Physical Principles and Sequence Design. 2014: Wiley.

7. Henderson, R.G., Nuclear magnetic resonance imaging: a review. Journal of the Royal Society of Medicine, 1983. 76(3): p. 206.

8. McRobbie, Donald W., MRI from Picture to Proton. 2007: Cambridge University Press.

9. Liney, G., MRI from A to Z: A Definitive Guide for Medical Professionals. 2010: Springer London.

10. MRI., Magnetic Resonance Imaging (MRI) Quality Control Manual: 2001. 2001: American College of Radiology.

11. Garber, K., Energy Boost: The Warburg Effect Returns in a New Theory of Cancer. Journal of the National Cancer Institute, 2004. 96(24): p. 1805-1806.

12. Feron, Olivier, Pyruvate into lactate and back: From the Warburg effect to symbiotic energy fuel exchange in cancer cells. Radiotherapy and Oncology, 2009. 92(3): p. 329-333.

13. Vander Heiden, Matthew G., Lewis C. Cantley, and Craig B. Thompson, Understanding the Warburg Effect: The Metabolic Requirements of Cell Proliferation. Science, 2009. 324(5930): p. 1029-1033.

14. Warburg, Otto, On the Origin of Cancer Cells. Science, 1956. 123(3191): p. 309-314.

15. Gatenby, Robert A. and Robert J. Gillies, Why do cancers have high aerobic glycolysis? Nat Rev Cancer, 2004. 4(11): p. 891-9.

16. Goldman, M., R. T. Schumacher, Spin temperature and nuclear magnetic resonance in solids. 1970: Clarendon Press Oxford.

17. Kurhanewicz, John, Daniel B. Vigneron, Kevin Brindle, Eduard Y. Chekmenev, Arnaud Comment, Charles H. Cunningham, Ralph J. Deberardinis, Gary G. Green, Martin O. Leach, Sunder S. Rajan, Rahim R. Rizi, Brian D. Ross, Warren S. Warren, and Craig R. Malloy, Analysis of Cancer Metabolism by Imaging Hyperpolarized Nuclei: Prospects for Translation to Clinical Research. Neoplasia, 2011. 13(2): p. 81-97.

18. Ardenkjaer-Larsen, J.H., B. Fridlund, A. Gram, G. Hansson, L. Hansson, M. H. Lerche, R. Servin, M. Thaning, and K. Golman, Increase in signal-to-noise ratio of > 10,000 times in liquid-state NMR. Proc Natl Acad Sci U S A, 2003. 100(18): p. 10158-63.

19. Abragam, A. and M. Goldman, Principles of dynamic nuclear polarisation. Reports on Progress in Physics, 1978. 41(3): p. 395.

20. Witney, T.H., M.I. Kettunen, and K.M. Brindle, Kinetic modeling of hyperpolarized 13C label exchange between pyruvate and lactate in tumor cells. J Biol Chem, 2011. 286(28): p. 24572-80.

21. Lumata, Lloyd, Chendong Yang, Mukundan Ragavan, Nicholas Carpenter, Ralph J. Deberardinis, and Matthew E. Merritt, Hyperpolarized 13C Magnetic Resonance and Its Use in Metabolic Assessment of Cultured Cells and Perfused Organs. Methods in Enzymology Metabolic Analysis Using Stable Isotopes, 2015: p. 73-106.

22. Bankson, J. A., C. M. Walker, M. S. Ramirez, W. Stefan, D. Fuentes, M. E. Merritt, J. Lee, V. C. Sandulache, Y. Chen, L. Phan, P.-C. Chou, A. Rao, S.-C. J. Yeung, M.-H. Lee, D. Schellingerhout, C. A. Conrad, C. Malloy, A. D. Sherry, S. Y. Lai, and J. D. Hazle, Kinetic Modeling and Constrained Reconstruction of Hyperpolarized [1-13C]-Pyruvate Offers Improved Metabolic Imaging of Tumors. Cancer Research, 2015. 75(22): p. 4708-4717.

23. Larson, Peder E. Z., Robert Bok, Adam B. Kerr, Michael Lustig, Simon Hu, Albert P. Chen, Sarah J. Nelson, John M. Pauly, John Kurhanewicz, and Daniel B. Vigneron, Investigation of Tumor Hyperpolarized [1-(13)C]-Pyruvate Dynamics Using Time-Resolved Multiband RF Excitation Echo-Planar MRSI. Magnetic resonance in medicine: official journal of the Society of Magnetic Resonance in Medicine / Society of Magnetic Resonance in Medicine, 2010. 63(3): p. 582-591.

24. Harris, T., G. Eliyahu, L. Frydman, and H. Degani, Kinetics of hyperpolarized 13C1-pyruvate transport and metabolism in living human breast cancer cells. Proceedings of the National Academy of Sciences, 2009. 106(43): p. 18131-18136.

25. Zierhut, Matthew L., Yi-Fen Yen, Albert P. Chen, Robert Bok, Mark J. Albers, Vickie Zhang, Jim Tropp, Ilwoo Park, Daniel B. Vigneron, John Kurhanewicz, Ralph E. Hurd, and Sarah

J. Nelson, Kinetic modeling of hyperpolarized 13C1-pyruvate metabolism in normal rats and TRAMP mice. Journal of Magnetic Resonance, 2010. 202(1): p. 85-92.

26. Bowen, Sean, and Christian Hilty, Rapid sample injection for hyperpolarized NMR spectroscopy. Physical Chemistry Chemical Physics, 2010. 12(22): p. 5766-5770.

27. Comment, A., B. Van Den Brandt, K. Uffmann, F. Kurdzesau, S. Jannin, J. A. Konter, P. Hautle, W. T. Wenckebach, R. Gruetter, and J. J. Van Der Klink, Principles of Operation of a DNP Prepolarizer Coupled to a Rodent MRI Scanner. Applied Magnetic Resonance, 2008. 34(3): p. 313-319.

28. Reynolds, Steven, Samira M. Kazan, Joanne E. Bluff, Michael Port, Emily Wholey, Gillian M. Tozer, and Martyn Paley, Fully MR-Compatible Syringe Pump for the Controllable Injection of Hyperpolarized Substrate in Animals. Applied Magnetic Resonance, 2012. 43(1-2): p. 263-273.

29. Reed, Galen D., Cornelius von Morze, Alan S. Verkman, Bertram L. Koelsch, Myriam M. Chaumeil, Michael Lustig, Sabrina M. Ronen, Jeff M. Sands, Peder E. Z. Larson, Zhen J. Wang, Jan Henrik Ardenkjær Larsen, John Kurhanewicz, and Daniel B. Vigneron, Imaging Renal Urea Handling in Rats at Millimeter Resolution Using Hyperpolarized Magnetic Resonance Relaxometry. Tomography 2.2, 2016: p. 125-37

8 Vita

Harlee Grace Harrison was born in Flowood, Mississippi on August 3, 1992, the daughter of George Michael Harrison and Jayna Cogdill Harrison. After graduating from University Christian School, Flowood, Mississippi in 2010 she entered The University of Mississippi in Oxford, Mississippi. She received Bachelor of Science degree with a major in Physics and a minor in Mathematics. In August of 2014 she entered the Medical Physics Master's program at The University of Texas Graduate School of Biomedical Sciences at Houston. On May 16, 2015 she married Preston Grant Griffin. After graduation, Harlee plans to continue her education by pursing a Doctorate of Medical Physics at the University of Texas Health and Science Center in San Antonio, Texas.